Davide Piovesan[1]
Department Biomedical Industrial and Systems Engineering,
Gannon University,
109 University Square,
Erie, PA 16541
e-mail: piovesan001@gannon.edu

Maxim Kolesnikov
Polaris Industries,
7290 E. Viking Boulevard,
Wyoming, MN 55092
e-mail: max.kolesnikov@polaris.com

Kevin Lynch
Department of Mechanical Engineering,
Northwestern University,
2145 Sheridan Road,
Evanston, IL 60208
e-mail: kmlynch@northwestern.edu

Ferdinando A. Mussa-Ivaldi
The Shirley Ryan Ability Lab,
355 E Erie Street,
Chicago, IL 60611;
Department of Physiology,
Northwestern University,
M211 303 E. Chicago Avenue,
Chicago, IL 60611
e-mail: sandro@northwestern.edu

The Concurrent Control of Motion and Contact Force in the Presence of Predictable Disturbances

The simultaneous control of force and motion is important in everyday activities when humans interact with objects. While many studies have analyzed the control of movement within a perturbing force field, few have investigated its dual aspects of controlling a contact force in nonisometric conditions. The mechanism by which the central nervous system controls forces during movements is still unclear, and it can be elucidated by estimating the mechanical properties of the arm during tasks with concurrent motion and contact force goals. We investigate how arm mechanics change when a force control task is accomplished during low-frequency positional perturbations of the arm. Contrary to many force regulation algorithms implemented in robotics, where contact impedance is decreased to reduce force fluctuations in response to position disturbances, we observed a steady increase of arm endpoint stiffness as the task progressed. Based on this evidence, we propose a theoretical framework suggesting that an internal model of the perturbing trajectory is formed. We observed that force regulation in the presence of predictable positional disturbances is implemented using a position control strategy together with the modulation of the endpoint stiffness magnitude, where the direction of the endpoint stiffness ellipse's major axis is oriented toward the desired force. [DOI: 10.1115/1.4044599]

Keywords: bio-inspired design, compliant mechanisms, control, dynamics, haptic devices, medical robotics, multibody dynamics and exoskelotons

Introduction

Recent experiments on neural activity in primates' motor and parietal cortex have suggested that there exist two separate modules for modulating motions and contact forces in the motor control system [1–5]. Several studies on human motor control have focused mainly on the control of movements, while little attention has been paid to the mechanisms underlying the control of contact forces.

Within the robotics literature, the dualism between force and position control has been the topic of several studies, producing a variety of hybrid position/force control schemes [6–11].

Impedance describes the resistive force of a mechanical system subject to a movement perturbation and characterizes the mechanics of human limbs when interacting with the environment. Early research on the modulation of impedance in humans [12] has progressed in the last 30 years, stressing the role of the central nervous system (CNS) in the modulation of impedance when interacting with unstable dynamics [13,14]. Furthermore, recent research suggests the existence of separate neural control mechanisms of hand movements and contact forces [3,15,16] and indicates that the segmental reflex feedback contributes to the regulation of position and force tasks [17].

Position control in humans is associated with an increase of impedance [18]. This is a way for the control system to reject random force perturbations that would deviate the hand movement. On the other hand, if the goal is to regulate the contact force in the presence of motion disturbances, an increase in compliance—i.e., a decrease of stiffness—would be the most effective strategy. There are neural and mechanical constraints—such as reflex delays, musculoskeletal mass, and muscle strengths—that limit the range of impedance that the motor system can attain. Experiments on reaching movements in the presence of deterministic forces, e.g., force fields, demonstrated that the CNS can compensate these type of perturbations by forming a predictive model of forces [19,20]. This is a good alternative for using feedback mechanisms that are prone to large time delays, but it is contingent upon the perturbation being predictable.

The goal of this work is to investigate the ability of the human CNS to control contact forces, while the arm is subject to a predictable external motion. This situation is dual to the compensation of predictable forces when the goal is a movement trajectory. We hypothesize that subjects would modulate their impedance as the experiment proceeds by choosing among different strategies to minimize the contact force errors. For this purpose, human subjects were asked to exert a force in a chosen direction while a planar sinusoidal motion of the hand was induced by a robotic device. We estimated the impedance modulation by applying small perturbations, and we observed that during force regulation in predictable environments, mechanical impedance increases while force production becomes more stable and the error in applied force decreases. The results of this study provide new evidence of the CNS' ability to control the exertion of force at the hand on a moving contact point, shedding some light on possible mechanisms adopted for the minimization of the interaction force errors. This result is a useful contribution in the ongoing debate regarding the controlled variables in human motor control [21–25].

Methods

Theoretical Hypotheses for Force Regulation. Force control regulates the exertion of a contact force in a specified direction.

[1]Corresponding author.
Contributed by the Mechanisms and Robotics Committee of ASME for publication in the Journal of Mechanisms and Robotics. Manuscript received February 26, 2019; final manuscript received July 30, 2019; published online September 9, 2019. Assoc. Editor: Nabil Simaan.

 Copyright © 2019 by ASME

An ideal force controller produces the force:

$$\mathbf{F} = \mathbf{F}_{\mathbf{ref}}(\mathbf{x}, \dot{\mathbf{x}}, t) \tag{1}$$

where $\mathbf{F}$ is the time-varying force produced by the controller and $\mathbf{F}_{\mathbf{ref}}$ is the reference force signal. We describe vectors in bold and scalars in italic.

A special case of force regulation sets

$$\mathbf{F}(\mathbf{x}, \dot{\mathbf{x}}, t) = \text{const} \tag{2}$$

Assuming $\mathbf{X}$ as the vector of generalized coordinates of the hand at the point of contact with the environment (e.g., Cartesian), to satisfy Eq. (2), one obvious condition is to ensure that

$$\frac{\partial \mathbf{F}}{\partial \mathbf{x}} = \frac{\partial \mathbf{F}}{\partial \dot{\mathbf{x}}} = \mathbf{0} \tag{3}$$

Defining $\mathbf{K} = \partial \mathbf{F}/\partial \mathbf{x}$ as the stiffness, experimental evidence shows that stiffness in humans is a function of the generalized coordinates, and in static conditions, it increases in magnitude with the muscle activation $\boldsymbol{u}(t)$ [26–33]. In practice, limb stiffness can never go below a basal threshold, which increases for high levels of the applied force, where muscle activation is also high. It should be noted that, during movement, activation and stiffness might not co-vary. During movement, the length of the muscle and its moment arm can change nonlinearly. If the moment arm decreases along a trajectory, the muscle force needs to be increased to maintain a constant stiffness, thus requiring an increase in activation [34]. Our objective is to clarify how the central nervous system can cope with these physiological aspects to achieve the condition in Eq. (2) when the contact point between the hand and the environment is moving (i.e., $\dot{\mathbf{x}} \neq \mathbf{0}$). To do that, we can analyze how a set of predictable dynamics of the environment can change the mechanics of the human.

A group of human subjects was asked to exert a constant force $\mathbf{F}(\mathbf{x}, \dot{\mathbf{x}}, t) = \text{const}$ in predefined directions while holding the end effector of a robotic device known as HapticMaster (HM) (FCS Control Systems, the Netherlands) [35]. The admittance-controlled robotic device was used to impose a movement to the hand of each subject. To impose the movement of the physical contact point $\mathbf{x}(t)$ between the HM and the human, the control of the robot reads the contact force $\mathbf{F}(\mathbf{x}, \dot{\mathbf{x}}, t)$ and commands a virtual motion $\mathbf{x_e}(t)$, which is transformed in the movement $\mathbf{x}(t)$ via a virtual impedance with mass $\mathbf{M_e}$, stiffness $\mathbf{K_e}$, and damping $\mathbf{B_e}$. Thus, the equation that describes the control of the robot is as follows:

$$\mathbf{M_e} \cdot \ddot{\mathbf{x}}_\mathbf{e} + \mathbf{B_e} \cdot (\dot{\mathbf{x}}_\mathbf{e} - \dot{\mathbf{x}}) + \mathbf{K_e}(\mathbf{x_e} - \mathbf{x}) = \mathbf{F}(\mathbf{x}, \dot{\mathbf{x}}, t) \tag{4}$$

Equally, the force at the contact point from the human side can be calculated using a similar equation:

$$\mathbf{M} \cdot \ddot{\mathbf{x}} + \mathbf{B} \cdot (\dot{\mathbf{x}} - \dot{\mathbf{x}}_{\mathbf{ref}}) + \mathbf{K} \cdot (\mathbf{x} - \mathbf{x}_{\mathbf{ref}}) + \mathbf{F}_{\mathbf{ref}}(t) = \mathbf{F}(\mathbf{x}, \dot{\mathbf{x}}, t) \tag{5}$$

where for the human limb, $\mathbf{M}$ is the inertial matrix, $\mathbf{B}$ is the damping matrix, $\mathbf{K}$ is the stiffness matrix, and $\mathbf{F}(\mathbf{x}, \dot{\mathbf{x}}, t)$ is the contact force. $\mathbf{F}_{\mathbf{ref}}(t)$ and $\mathbf{x}_{\mathbf{ref}}(t)$ are the reference force and trajectory, respectively, imposed by the CNS to accomplish the task. In principle, these two variables could be controlled independently along two independent directions (e.g., imposing $\mathbf{x}_{\mathbf{ref}}(t)$ along its y component and $\mathbf{F}_{\mathbf{ref}}(t)$ along x). Notice that Eqs. (4) and (5) are linearized with respect to the position of the hand and are only valid in a small neighborhood of such position. This is important to guarantee that coefficients $\mathbf{M}$, $\mathbf{M_e}$, $\mathbf{B}$, $\mathbf{B_e}$, $\mathbf{K}$, and $\mathbf{K_e}$ are constant within the neighborhood. Equations (4) and (5) are obviously systems with two degrees of freedom (2-DOF). A simplified example for a single degree of freedom can be observed (Fig. 1(*a*)), where "x" is the common contact point between the human and the robot, calculated with respect to a common ground. Furthermore, to be in equilibrium, the contact force from the robot side needs to be the same as the one of the human side. The force F between the ground and x for the robot side can be calculated using Eq. (4), where the inertial force caused by M_e depends

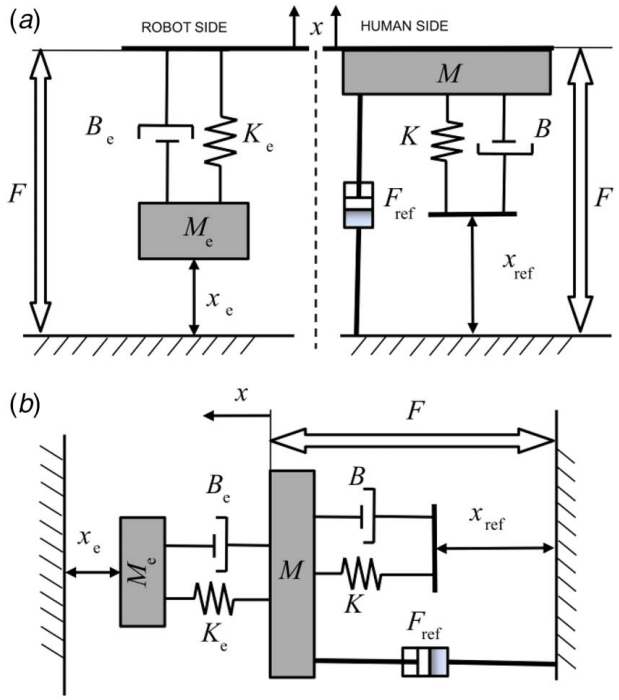

Fig. 1 (*a*) Representation of the arm and the robot as mechanical systems for the direction of applied motion (*x*) and (*b*) representation of couples system

on the second derivative of x_e with respect to time. The viscoelastic force depends on the difference between x and x_e and its first derivative with respect to time. The same force, from the human side, can be calculated with Eq. (5), where the inertial force caused by M depends on the second derivative of x with respect to time. The viscoelastic force depends on the difference between x and x_{ref} and its first derivative with respect to time. F_{ref} is added in parallel.

To simplify our experiment, we analyzed a set of tasks in which force generation and imposed movement are either parallel or orthogonal. This can largely simplify Eqs. (4) and (5) that, as a system, will reflect the dynamics of the coupled mechanical system in Fig. 1(*b*).

The generation of force by the human in a specific direction can be therefore represented by the following scalar equation:

$$F = \frac{Z_e}{Z_e + Z} \cdot (Z \cdot (v_e - v_{\text{ref}}) + F_{\text{ref}}) \tag{6}$$

where Z_e is the impedance of the environment in the direction of force application, Z is the impedance of the human arm in the same direction, and the transform of reference force and reference velocity v_{ref} and F_{ref} are parameters that can be modified by the CNS. An explanation of how Eq. (6) is derived is included in Appendix A.

Equation (6) can be used conveniently to test which different force control strategies the human could utilize. The strategies are summarized as follows:

(1) *Classical force control*: This control architecture decreases the arm impedance Z so that if $Z \to 0$, Eq. (6) yields $F \to F_{\text{ref}}$. Notice that the only objective of this architecture is to control the contact force. Position is not controlled, and any disturbance to the end effector would produce very little variation of force but may create large variations of the position [7]. Instability is not a problem in this experiment since the subject is interacting with an imposed movement of the robot. Therefore, subjects have the option to decrease stiffness without being concerned with mechanical

instability of the end effector and use a mechanism that simply modulates F_{ref}.

(2) *Hybrid position/force control*: Assuming that both kinematic and force references exist, the advantage of hybrid control is that the position and force information are analyzed independently to take advantage of well-known control techniques for each case [36]. The torque at the joints can be compartmentalized by the two separate controllers and are combined only at the final stage. The positional part of the controller can generate a perfect match between v_{ref} and v_e compensating for the kinematic. The perfect velocity match in Eq. (6) will produce a contact force equal to $F = \frac{Z_e}{Z_e+Z} \cdot (F_{ref})$. This implies that even with a perfect position control, the impedance of the arm needs to be very low in order to have a good match between the reference force F_{ref} and the force exerted on the environment F.

(3) *Classical impedance control*: As suggested by Hogan [7], an impedance controller must specify two variables (i.e., position and impedance) in order to obtain the contact force required by the task. The impedance must contain a static component (i.e., stiffness) in order to maintain stability if the impedance of the environment is negligible. By setting the motion plan to $v_{ref} = v_e - v_0$, where v_0 is an arbitrary velocity of the hand, we can completely compensate for the motion of the environment and impose an additional movement to the contact point to obtain the desired force even if a direct control of force is not present ($F_{ref} = 0$). Here:

$$F = \frac{Z_e \cdot Z}{Z_e + Z} \cdot v_0 \tag{7}$$

The advantage of classical impedance control is in its inherent stability; however, it requires a priori knowledge of the movements of the contact point, and it is difficult to use in nonstructured environments. In its simplest form, impedance control is a position controller where stiffness and damping of the arm can be regulated to obtain the desired force. Unfortunately, if stiffness and damping are kept constant at the joint level, the Cartesian impedance at the hand will change with the arm configuration due to the strong nonlinearity of the arm kinematics. This produces the inability to follow a command force trajectory unless a representation of the inverse kinematics is part of the controller.

(4) *Hybrid impedance/force control*: In both force and hybrid force/position architectures, the control strategy is specified as a trajectory tracking problem (i.e., tracking a given motion and/or force trajectory). Impedance control assumes a tracking of motion and a desired impedance to match the desired force [37]. Yet, as shown in Eq. (7), any variation of the impedance of the environment will generate a change in force. This requires the capability of the system to estimate the physical properties of the environment and a very precise control of position to compensate for any rapid change. The possibility to use two controls in parallel, such as impedance control and force control, allows for a stable system (the principal features of impedance control) and for the necessity of predicting only the position of the hand. Indeed, the force controller could rapidly compensate any force error without predicting the environmental impedance and without an internal representation of the inverse kinematics to change the arm impedance as a function of the arm configuration.

Our experimental approach aims at determining which of the aforementioned control strategies are most likely to be employed by the human CNS to regulate contact forces or at least to exclude those that are deemed unlikely. Based on the four architectures, the direct measure of subjects' arm impedance (evaluated in the same arm configuration for each subject) provides an indicator to assess which control strategy has likely been utilized. If the impedance is low or decreases over time, we can expect either a force control or a hybrid position/force control strategy. If the strategy is to maintain high impedance, in the measured position, we might be in the presence of an impedance control. It is impossible to distinguish between impedance control and hybrid impedance/force control unless a change in the impedance of the environment occurs. In the latter case, since a prediction of the environment is not necessary, the impedance could remain constant letting the force control compensate for the variation of contact forces. On the other hand, by using an impedance control, we should see a change in impedance over time.

Participants. Ten right-handed subjects (seven males and three females, aged 21–36 years) participated in the experiment. Every participant reported a normal or corrected to normal vision, a normal sense of touch, and no known history of neurological disorders. The experiment was approved by the Institutional Review Board of Northwestern University.

Apparatus. Visual information was displayed on a Dell 1907FPc 19" LCD monitor (Dell Inc., Round Rock, TX) placed approximately 110 cm from the user. Haptic guidance was presented via a HM robotic manipulator (FCS Control Systems, the Netherlands) [35] placed in front of the subjects. Participants were asked to hold the handle of the manipulator with their right arm and to place their elbow on an armrest. The armrest compensates gravity but allows free motion in the plane. The height of the armrest was adjusted for each subject individually, so that the shoulder, elbow, and wrist joints were situated in a horizontal plane. Figure 2 depicts the experimental setup. The shoulder and elbow position were 15 deg and 115 deg, respectively.

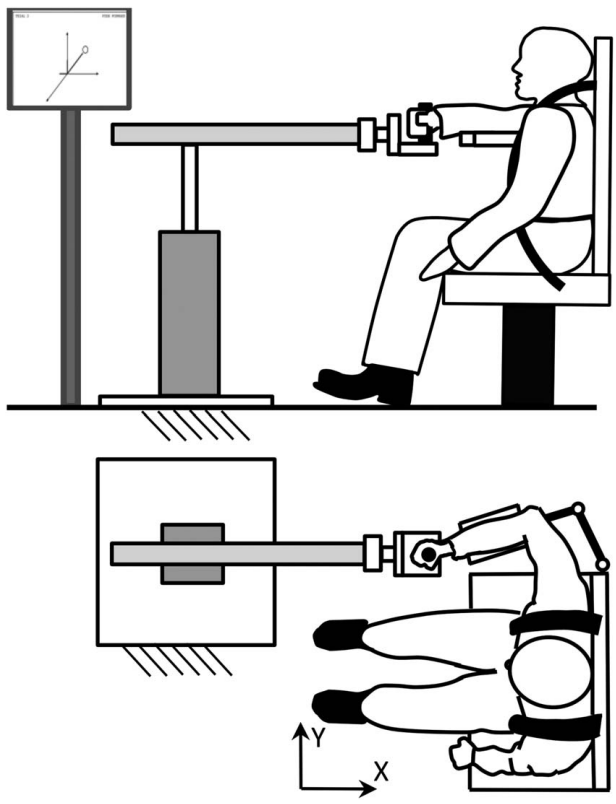

Fig. 2 Position of the subject during the experiment. Force regulation was constrained on the *x-y* plane. Subjects received a visual feedback of the applied force on a display, representing the force vector applied and the force target to be reached. The FD is –*x*.

The software used for this experiment was developed in C++ using the proprietary HapticMaster API (FCS Control Systems). Visual feedback presented to the user was developed in OPENGL API (Khronos Group, Beaverton, OR) and incorporated into the experimental software. The endpoint was virtually connected to the mass of 5 kg by way of spring and damper dynamics (stiffness: 10 kN/m with critical damping of 447.21 Ns/m). Position, velocity, and force were recorded using the embedded instrumentation of the robot.

Experimental Task. The axis convention used in this study reflects the HM frame of reference where the x-axis runs toward the participant, the y-axis runs medially to laterally, and the z-axis runs from the bottom to the top. The experiment is carried out on the plane $z = 0$.

The task chosen for this experiment was to produce an isometric force of $|\mathbf{F}| = 10N$ at the handle of the HM in the four principal Cartesian directions in the horizontal plane. Three-dimensional graphical feedback of the applied force was always provided to the subject. A displacement applied to the hand will generally generate a reaction force whose direction is a function of arm mechanics. The position of the hand was not displayed on the monitor. The position of the subject and the user's view of the computer monitor are shown in Fig. 2.

Each participant was first introduced to the device and verbally instructed on the experimental task. We asked the subject to generate a force in the indicated direction regardless of the robot actions, without giving any instruction on how to compensate for external disturbances.

In the first part of the trial, the handle was stationary, and the user simply had to match the produced force with the reference force $\mathbf{F} = \mathbf{F_{ref}}$ represented by a circular target on the screen. The target was located in the direction of force application at 10 cm distance from the origin of a three-dimensional frame represented in the dimetric projection (Fig. 2). As an example, assuming that the direction of force application (FD) is the x-axis, the force reference vector is $\mathbf{F}_{\text{ref}} = \begin{bmatrix} F_{\text{ref}} & 0 & 0 \end{bmatrix}^T$. Subjects were to maintain the force in the direction of application within a threshold δ so that $F \subset (F_{\text{ref}} - \delta,\ F_{\text{ref}} + \delta)$. The force components along the other two unloaded axes had to stay in the interval $(-\delta,+\delta)$. The threshold parameter was chosen as $\delta = 0.1 \cdot F_{\text{ref}}$. When forces in all three directions were within their respective thresholds, the force cursor changed its color to green.

When the subject was able to successfully maintain the target force while satisfying these conditions for 5 s, the second part of the trial commenced. In this part, the handle of the manipulator moved sinusoidally about the center position along one specific direction (either the x- or y-axis) with the semi-amplitude of 10 cm and frequency of 0.125 Hz for $N_c = 25$ cycles. Based on these parameters, each trial lasted 200 s. The subject was asked to maintain the same reference force while the movement was under way. Each subject completed $N_T = 8$ trials consisting of all possible combinations of four planar principal directions of force production and two axes of periodic motion. With reference to Fig. 3, we defined the following labels for each experimental condition (i.e., task), where the first letter indicates the direction of the force, the sign represents its orientation, and the second letter indicates the axis of the movement (the sign for the movement is not included as the oscillation occurs alternatively in the positive and negative direction):

$$+XX, -XX, \ +YX, -YX, +XY, -XY, +YY, -YY$$

Impedance Estimation. To understand the strategy that the CNS is using to accomplish the task, we estimated the arm mechanics at the endpoint using a 2-DOF planar model of the arm [38,39].

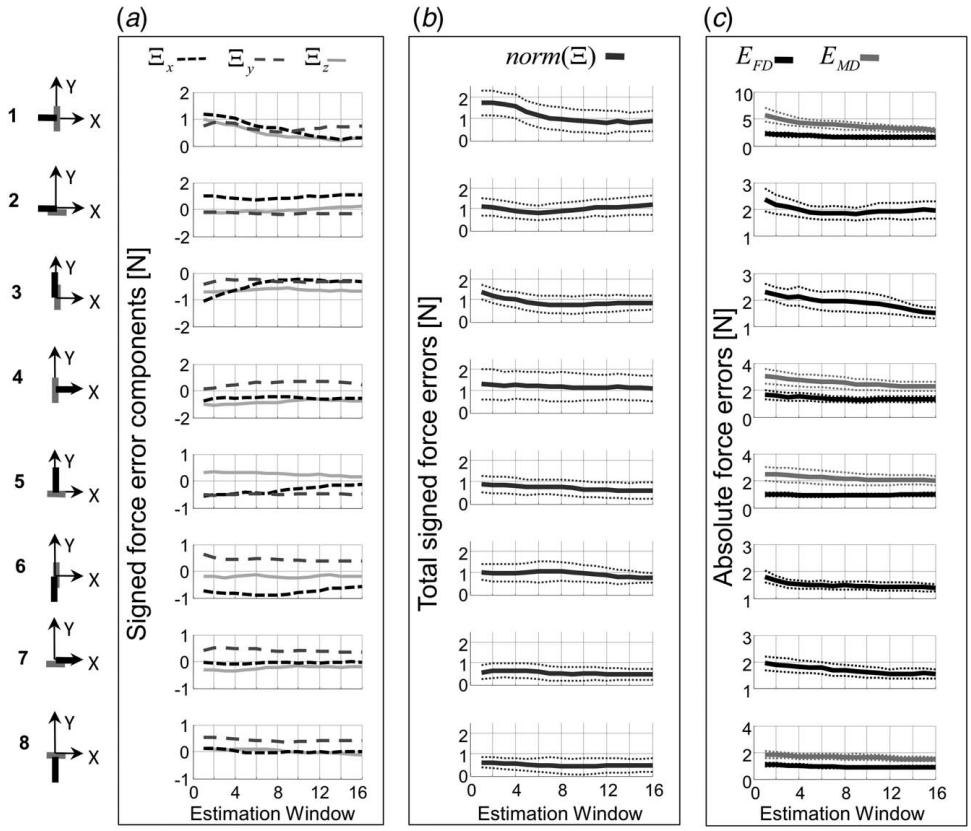

Fig. 3 Force errors exerted during each experimental condition: (*a*) signed error for each direction in the Cartesian space. In the top part, the different line patterns adopted for each Cartesian direction are shown. (*b*) Norm of signed errors. (*c*) Absolute error in the direction of force (FD) and in the direction of movement (MD).

Endpoint stiffness was estimated from position perturbations of amplitude 8 mm and duration of 300 ms, applied twice per movement cycle at the points of zero acceleration. The perturbation's profile encompassed a short transition phase of 100 ms at the start and at the end, obtained using a sixth-order polynomial constrained by zero velocity and zero acceleration at both boundaries and zero end jerk (minimum snap trajectory) [40]. The direction of each perturbation was randomly chosen from the set $\left\{\frac{k\pi}{4} \mid k = 1, 2, \ldots, 8\right\}$, with 0 aligned with the x-axis.

The total number of perturbations encountered by each participant during every trial was $N_P = 50$, i.e., 25 cycles with 2 perturbations per cycles, always when $x = y = 0$, but one when the hand was moving from the positive to the negative coordinate, while the other when moving from the negative to the positive coordinate. Most participants were not aware of the existence of these perturbations due to their low amplitude and extremely short duration. Others who were aware of it tended to attribute their effect to "imperfections" of the equipment.

The inertia is a geometrical characteristic of the limb, and it is invariant in the 2-DOF model since the estimations occur in the same joint configuration. On the other hand, stiffness and damping depend on passive joint properties [41,42], volitional interventions [43], and the reflex pathways responsible for the alteration of muscle activation [44,45]. As such, stiffness and damping provide a complete characterization of the mechanical properties of the limb that can be directly modulated by neural activities. To reduce the number of parameters estimated at once, we evaluated the endpoint stiffness and damping using a linear multivariate regression, where the inertial properties of the arm were computed separately [38,39,46]. The joint inertial parameters were calculated for each subject by means of nine estimation methods (Hanavan (HV) [47], Dempster (DE) [48], Chandler (CH) [49], Clauser (CL) [50],McConville (MC) [51], Zatsiorsky and Seluyanov (Z1) [52], Piovesan (PI) [53], Zatsiorsky and Seluyanov (Z2) [54], and de Leva (DL) [55]).

Each model suggested a series of limb and anthropometric dimensions to input in the regressive equations required to obtain the inertial parameters at the joint level. Method HV is based on the approximation of the geometry of the limb with 3D basic geometric shapes. Methods DE, CH, and CL are commonly used and derived the estimation of arm parameters from cadaver dissections. Method MC determined the geometric properties of the arm from in vivo photographic images. Methods Z1 and Z2 are based on in vivo scans performed using gamma rays to determine the distribution of density. Method DL is an adjustment of methods Z1 and Z2, considering a slightly different segmentation of the arm. A detailed comparison between the aforementioned methods and a description of the water immersion method PI can be found in Ref. [53].

Inertial joint parameters were then transformed to the Cartesian endpoint space by means of the Jacobian matrix calculated for each subject.

We calculated the regression between the kinematic variables of the net perturbation and the force generated by it after subtracting the inertial force. The inertial force is obtained by multiplying the endpoint inertial matrix $\hat{\mathbf{M}}$ (estimated as the average of the nine methods described above) by the net perturbation acceleration.

Referring to Fig. 4, we can observe an example in which the movement of the hand is along the y-axis (the x-axis is set to $x = 0$), and the ith perturbation in both x and y directions is applied. To estimate the baseline of both the position and the force, we used a linear interpolation of the signal (straight line in Fig. 4) connecting the signal at time $t_0^i = 0s$ (first vertical line crossing time zero in Fig. 4) when the perturbation is applied to the time $t_f^i = t_0^i + 0.7s$ (vertical dashed line in Fig. 4). The error between $\mathbf{x}$ and $\mathbf{x_{ref}}$ (where both variables represent a vector of the trajectories in x and y) and its derivatives with respect to time is here identified with the vector "$\mathbf{e}$" and its derivatives with respect to time. The difference in force between the baseline force and the actual force is defined as $\Delta\mathbf{F_i}$.

To obtain a stable estimate of stiffness and damping, movement cycles are divided into blocks of size $N_w = 10$ cycles. Each block of 10 consecutive cycles is called a "window," and it is used for a single stiffness and damping estimate where the number of random perturbations for each estimate is $N_{Pw} = 2 \cdot N_w = 20$. Each ith perturbation ($i = 1..N_{Pw}$) encompassed 300 ms worth of data from $t_0^i = 0s$ to $t_p^i = 0.30s$ (second red line in Fig. 4), so that the following regression equation can be used to estimate stiffness and damping within the jth block of 10 consecutive cycles:

$$\begin{bmatrix} \Delta\mathbf{F}_1 \\ \vdots \\ \Delta\mathbf{F_i} \\ \vdots \\ \Delta\mathbf{F}_{\mathbf{N_{P_w}}} \end{bmatrix}_{\mathbf{j}} - \hat{\mathbf{M}} \begin{bmatrix} \ddot{\mathbf{e}}_1 \\ \vdots \\ \ddot{\mathbf{e}}_{\mathbf{i}} \\ \vdots \\ \ddot{\mathbf{e}}_{\mathbf{N_{P_w}}} \end{bmatrix}_{\mathbf{j}} = \begin{bmatrix} \mathbf{K} & \mathbf{B} \end{bmatrix}_j \begin{bmatrix} \begin{bmatrix} \mathbf{e} \\ \dot{\mathbf{e}} \end{bmatrix}_1 \\ \vdots \\ \begin{bmatrix} \mathbf{e} \\ \dot{\mathbf{e}} \end{bmatrix}_i \\ \vdots \\ \begin{bmatrix} \mathbf{e} \\ \dot{\mathbf{e}} \end{bmatrix}_{\mathbf{N_{P_w}}} \end{bmatrix}_j$$

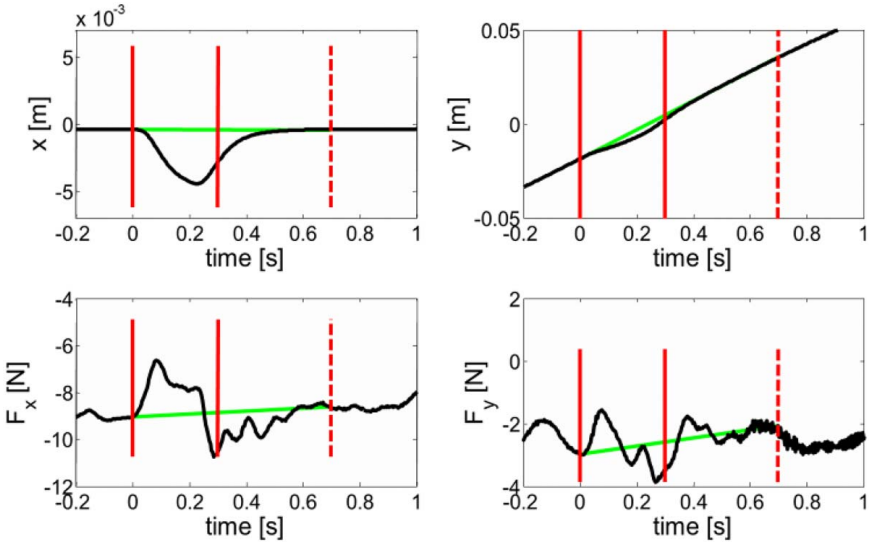

Fig. 4 Force errors exerted during each experimental condition. Signed error for each direction in the Cartesian space.

$$\left[\begin{bmatrix}\Delta\mathbf{F}_1\\ \vdots\\ \Delta\mathbf{F}_i\\ \vdots\\ \Delta\mathbf{F}_{N_{Pw}}\end{bmatrix}_j - \hat{\mathbf{M}}\begin{bmatrix}\ddot{\mathbf{e}}_1\\ \vdots\\ \ddot{\mathbf{e}}_i\\ \vdots\\ \ddot{\mathbf{e}}_{N_{Pw}}\end{bmatrix}_j\right]\begin{bmatrix}\begin{bmatrix}\mathbf{e}\\ \dot{\mathbf{e}}\end{bmatrix}_1\\ \vdots\\ \begin{bmatrix}\mathbf{e}\\ \dot{\mathbf{e}}\end{bmatrix}_i\\ \vdots\\ \begin{bmatrix}\mathbf{e}\\ \dot{\mathbf{e}}\end{bmatrix}_{N_{Pw}}\end{bmatrix}_j^{\#} = \begin{bmatrix}\mathbf{K} & \mathbf{B}\end{bmatrix}_j$$

Note that the symbol # represents the Moore–Penrose pseudoinverse of the kinematic errors in the jth window. To obtain the subsequent estimate for the $(j+1)$th window, we consider the next 10 consecutive cycles after the first (i.e., $j=(2..11)$). Given the number of movement cycles in the experiment ($N_c=25$), the maximum number of block estimates per trial is $N_{WT}=N_c-(N_w-1)=16$. Starting from the initial block estimate, we observed the evolution of stiffness and damping throughout the trial to identify the strategy adopted by each subject.

We used the canonical correlation to quantify the overall measure of linear association between kinematics and kinetics variables [56]:

$$r_I^2 = \max\left(eig(\boldsymbol{S}_{\boldsymbol{FF}}^{-1}S_{FX}\boldsymbol{S}_{\boldsymbol{XX}}^{-1}S_{XF})\right) \tag{8}$$

where $\boldsymbol{S}_{\boldsymbol{FF}}$ is the covariance matrix of the force generated by the perturbation, and $\boldsymbol{S}_{\boldsymbol{XX}}$ is the covariance matrix of the perturbation kinematics (position and velocity).

Hand acceleration was obtained as the first derivative of the velocity signal. Signals were filtered using a sixth-order Savitzky–Golay polynomial filter with a cutoff frequency of 23.4 Hz [57]. Since the movement of the hand is servo-commanded, there is no need to compute the intended trajectory of the hand as given in Ref. [13,58]. Within each perturbation, we subtracted the mean force to avoid bias.

Data Collection. Force and motion data were collected at a rate of 250 Hz. Each task performance trial was analyzed individually offline, and the average force and force errors were calculated using the following procedures.

The average force and absolute average errors for each cycle were calculated as follows:

$$\phi_s^k = \frac{1}{N}\sum_{\substack{n=1\\ n\notin P}}^{N} F_s(n) \tag{9a}$$

$$e_s^k = \frac{1}{N}\sum_{\substack{n=1\\ n\notin P}}^{N} |F_s(n) - F_{ref_s}(n)| \tag{9b}$$

where $F_s(n)$ is the force exerted along an arbitrary direction s among (x, y, z), N is the number of data points n collected during the kth cycle, not including the set of data points P collected when random perturbations were applied, and depends on the sampling frequency at which the force signal was acquired by the HapticMaster Robot.

Given the difference between the force $F_s(n)$ and the reference force $F_{ref_s}(n)$ in the same direction, the average absolute error e_s^k is calculated as the average of the absolute of such difference during the kth movement cycle. The value of the absolute error within a cycle always satisfies $e_s^k \geq 0$ with equality if and only if the actual and desired force trajectories coincide, i.e., $F(n)=F_{\text{ref}}(n) \quad \forall n \in N$.

The force error measures E_s^i and Ξ_s^i on the ith window are computed as follows:

$$\Xi_s^i = \left(\frac{1}{N_w}\sum_{j=1}^{N_w}\phi_s^{i+j-1}\right) - F_{ref_s} \quad | \quad i=1, 2, \ldots, N_{WT} \tag{10a}$$

$$E_s^i = \frac{1}{N_w}\sum_{j=1}^{N_w} e_s^{i+j-1} \tag{10b}$$

The signed force error Ξ_s^i for the direction s is the difference between the average force within the estimation window i and the reference force. Notice that since the average force ϕ_s^k can change sign from cycle to cycle, the error Ξ_s^i has a sign. Thus, we can observe whether subjects employ a continuous correction strategy to obtain the desired force or if there is a bias where the desired force is systematically undershot or overshot. On the other hand, the average force error E_s^i for the direction s in the window i is a measure of absolute force mismatch, which is useful to compare if the force error is independent from the direction of the movement.

Effectiveness of training is assessed by computing the skill gain G for each trial as a difference between the absolute force error measures of the last and first window:

$$G_s = E_s^1 - E_s^{N_{WT}} \tag{11}$$

Positive skill gain indicates improvement in the subject's performance during the trial, whereas negative skill gain indicates decline in performance. Larger reductions in the force error measures from the first window to the last window correspond to larger skill gains and greater effectiveness of the training for that particular subject.

Two kinds of force error are considered based on the characteristics of the direction s: the force error in the direction of motion (MD) and the force error in the direction of applied force (FD). For some trials, these two directions coincide. We denote the two kinds of skill gain values by G_{MD} and G_{FD}.

Of four components of the endpoint stiffness matrix $\mathbf{K}=\begin{bmatrix}K_{xx} & K_{xy}\\ K_{yx} & K_{yy}\end{bmatrix}$, two are of particular interest for our analysis. The first component of the stiffness we are interested in relates the displacement in the MD to the force in the MD. We call this component stiffness in the MD (K_{MD}). The second component of interest is the stiffness component relating the displacement in the MD to the force in the FD. We call this component stiffness in the FD (K_{FD}). If the two directions coincide, then $K_{FD}=K_{MD}$.

Stiffness modulation is assessed by calculating for each trial the difference between the stiffness estimates of the last and first blocks cycles:

$$\Delta K = K_{N_{WT}} - K_1 \tag{12}$$

This computation is performed for stiffness estimates in both the MD and the FD yielding the values of ΔK_{MD} and ΔK_{FD}.

To determine the relationship between each skill gain value and the corresponding change in stiffness, a simple correlation metric was used, which took into account only the sign of each variable:

$$R = \frac{1}{N_T}\sum_{i=1}^{N_T}\text{sgn}(G_i)\text{sgn}(\Delta K_i) \tag{13}$$

where G_i and ΔK_i denote the skill gain and stiffness modulation during the ith trial. Note that $-1\leq R\leq 1$ in all cases. The choice of this particular correlation metric instead of a linear correlation or other popular correlation metrics is motivated by an unknown and possibly nonlinear nature of the relationship between the two variables.

Statistical Analysis. Each coefficient of stiffness K_{ij} and damping B_{ij} is obtained as the regression slope between the kinetic variables i and the kinematic variables j. Since two dependent variables (i.e., total force minus inertial force in x and y) and four covariates (position and velocity for x and y) are present, a multivariate analysis needs to be performed. We test if each coefficient is statistically different from the beginning to the end of each force/movement condition.

Each regression coefficient represents the most probable value of a slope between dependent variables and covariates where a

variance is also associated with it. We need to establish if the regressions slopes representing each component of the impedance are different between the first and the last window estimate. Given two regression coefficients, obtained using the same variables and covariates although in two different period of the exercise (i.e., beginning and end), we can compare their statistical differences by means of a multivariate analysis of covariance (MANCOVA), which establishes if the regression slope is statistically different between the two groups. Thus, we need to estimate if the interaction effect between two groups (i.e., the first and the last window estimate) and the respective kinematic variables is significant.

Following the aforementioned procedure, we can also ascertain if the curl of each stiffness and damping matrix is statistically significant by determining if the slopes defining the terms outside of the diagonal are statistically different with respect to each other.

We analyzed the average stiffness and damping estimated among all inertial models for the human subjects in each experimental condition. The significant difference of the matrices' coefficients between the first and last window estimate of each experimental condition was tested using MANCOVA, where group (first versus last window estimate) was a fixed factor and "subjects" was a random factor. This analysis identified if the change in stiffness and damping along the MD and FD was significant between the beginning and end of each exercise.

We tested the effect of training on the matrix determinant and rotation angle metrics within each experimental condition. The effect of the inertial models was evaluated using a three-way repeated measures analysis of variance (ANOVA) with inertial models and window estimate as fixed factors and subjects as a random factor.

To analyze the curl within each experimental condition, we performed a four-factor ANOVA (subjects as random factor and window estimate, inertial method, and position outside the diagonal as fixed factors) between the terms xy and yx of both K and Z. A significant difference of the factor "position outside the diagonal" implies a statistically significant curl.

A similar analysis was performed among all experimental conditions to test if the subjects reoriented the stiffness in either MD or FD (four-factor ANOVA: subjects as random factor and window estimate, inertial method, and experimental condition as fixed factors).

The statistical significance of skill gain was tested for each experimental condition using a two-way ANOVA with window estimates as a fixed factor and subject as a random factor. The significance of the correlation between the skill gain and the change in impedance was evaluated using a sign test.

To test the influence of the method on the measurement, we replicated the experiment on a mechanical rig. The results obtained with the calibrated physical prototype are reported in Appendix B and indicated that the method can influence the estimation with an error up to 2.7%. Since the stiffness variation monitored in the human subjects was larger than that, it is quite unlikely that such variation would be an artifact of the technique or the result of noisy estimates.

Results

With Practice Subjects Learn to Produce More Accurate Contact Force. To confirm that subjects are able to control forces, it is important to establish that learning occurs and a reduction of force errors is taking place during the exercise.

Figure 3(*a*) shows the average among subjects of the signed error Ξ in the three cardinal directions. We can notice that by observing the signed error for each cardinal direction separately calculated as in Eq. (10*a*), there is not a preferential tendency to overshoot or undershoot the required force. On the other hand, by analyzing the norm of the signed error in Fig. 3(*b*), we can notice a general tendency for the error to decrease from the beginning to the end of training, as evidence that learning is taking place.

We can see in Fig. 3(*c*) that the absolute force error decreased both in the direction of movement (MD) and in the direction of force (FD) as each exercise progressed. While subjects were able to maintain a 10 N force magnitude accurately, when the MD was orthogonal to the FD, the absolute force errors in the MD were higher than the absolute force errors in the FD ($E_{MD} > E_{FD}$). As an example, for condition "1" (MD = y, FD = $-x$) in Fig. 3(*c*), the absolute average force error among subjects in the direction of movement is almost one third of the desired target force in the direction of force. A nonmonotonic behavior was observed in condition 2 (MD = x, FD = $-x$), where the force error decreased considerably within the first eight window estimates, but then increased to a value similar to the initial. A separate analysis was conducted for each experimental condition (two-way repeated measures ANOVA: window estimates as fixed factor and subject as a random factor) to evaluate the effect of force learning within each condition. In the majority of conditions, the skill gains G_{MD} and G_{FD} increased (i.e., a reduction in force errors between the first and last window estimate as defined in Eq. (11)) as the training progressed, showing evidence of learning. Increases in skill gains were significant ($p < 0.01$) or marginally significant (threshold $0.01 < p < 0.08$), as given in Table 1.

Stiffness and Impedance Magnitude and Orientation. The determinant of the stiffness and the determinant of the impedance at the frequency of the movement were almost identical (Fig. 5). This is an indication that the system is dominated by the stiffness. This condition is desirable for the study of force control as the impedance could be decreased to low values voluntarily just by modulating the stiffness. We can notice that the determinant of the damping component is negligible.

Our analysis shows that the stiffness orientation is statistically different across experimental conditions ($p < 0.0001$). Figure 5 shows that the orientation of impedance (and therefore stiffness since it is its predominant component) changes with respect to the direction of the force. The major axis of the impedance ellipse is on average 30 deg when the force is directed along the x-axis (0 deg being the direction of x). When the force requirement is along the y-axis, the average angle is significantly bigger (45 deg) showing a marked shift toward the direction of the force independent of the direction of the movement. We used a single-way ANOVA with the direction of force as a factor. The change in orientation, even though not dramatic, was statistically significant ($p < 0.0001$) and compatible with the voluntary change in stiffness orientation described by Perreault et al. [32].

Stiffness and Impedance Increase as Force Error Decreases. Figure 6 shows the ellipses of stiffness, the ellipses of damping, and

Table 1 Analysis of variance with subject as a random factor for force error in the direction of motion (MD) and in the direction of force (FD)

	1		2		3		4		5		6		7		8	
	F	p	F	p	F	p	F	p	F	p	F	p	F	p	F	p
G_M	3.33	**0.00**	0.59	0.88	3.13	**0.00**	3.65	**0.00**	1.74	0.05	3.35	**0.00**	4.78	**0.00**	1.59	0.08
G_F	3.10	**0.00**	0.59	0.88	3.13	**0.00**	1.94	**0.01**	0.43	0.97	3.35	**0.00**	4.78	**0.00**	1.40	0.15

$p < 0.01$ is indicated in bold.

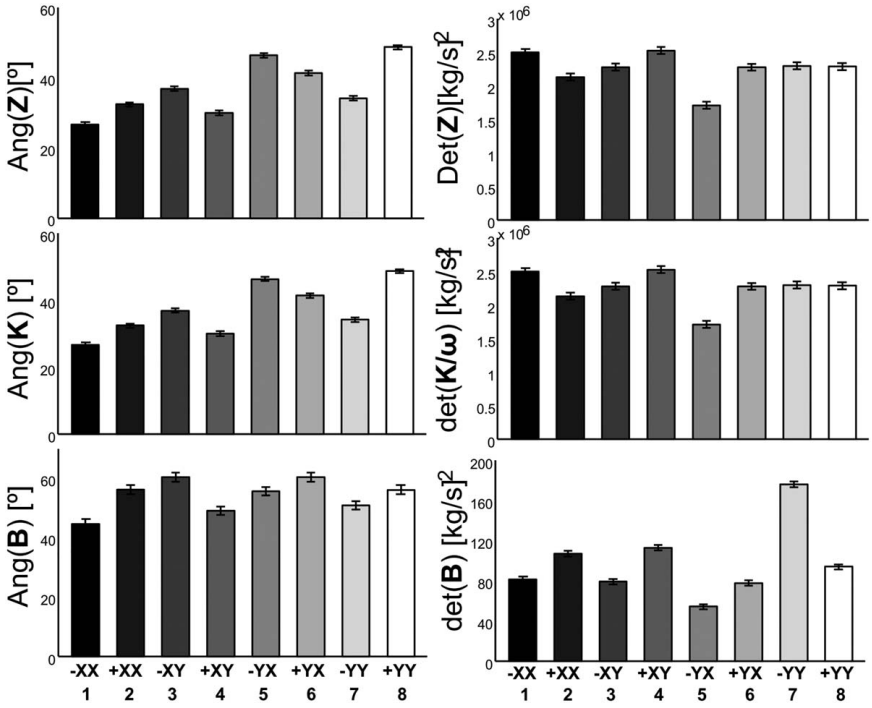

Fig. 5 Determinant and orientation of total impedance (*Z*), stiffness (*K*), and damping (*B*) ellipses at the frequency of the movement ($f = 0.125$ Hz). The orientation of the ellipses is calculated considering the major axis at 0 deg when aligned in the *x* direction as illustrated in Fig. 1.

the ellipses of impedance at the frequency of the movement (0.125 Hz) for all the experimental conditions as an average of all ten participants. The canonical correlation indicates how well the system is approximated by a linear relationship between input and output. The canonical correlation across subjects and conditions is $r_I^2 = 0.80$, indicating a modest nonlinearity between kinetic and kinematic variables.

The variation of stiffness matrix rotation during the adaptation is insignificant or marginally significant for cases 3 (MD = *y*, FD = +*y*) and 4 (MD = *y*, FD = +*x*). In the latter case, the change in rotation is less than 6 deg. The significance of each parameter variation for both stiffness and impedance is reported in Table 2. Figure 6 also highlights the monotonic increase in stiffness, damping, and impedance magnitude as the experiment progresses. This can be observed by the general increase in area of the ellipses. There is a statistically significant increase in the stiffness and impedance determinant between the beginning and the end of each experimental condition as represented in Table 2.

Evolution of the overall stiffness magnitude expressed by det(**K**) [12], curl, and orientation variation within each experimental condition is also presented in Fig. 7(*d*). As reported in Table 3, the terms outside of the matrices diagonal are never statistically different from each other for both stiffness and impedance, showing that the curl is not statistically different from zero.

We calculated both the impedance and stiffness matrices for each subject using nine different inertial models. Table 4 shows MANCOVA for the average of each stiffness/impedance coefficient across inertial models calculated on the whole subject population between the first and the last estimating window of each experimental condition. We can observe the significant change of the terms on the diagonal for both the stiffness matrix and the impedance matrix. Moreover, the off-diagonal terms did not statistically change in the majority of the cases. Since both K_{xx} and K_{yy} were statistically different between the first and the last window estimate, so were the values of ΔK_{MD} (difference in stiffness along MD) and ΔK_{FD} (difference in stiffness along FD), which are depicted in Fig. 7(*b*).

Skill gains averaged for each condition across subjects are depicted in Fig. 7(*a*). "#" indicates elements that were marginally significant ($0.01 < p < 0.08$), and "@"indicates nonsignificant cases.

Correlation coefficients for every subject computed according to Eq. (13) (see "Methods section") are presented in Fig. 7(*c*). The majority of subjects exhibited positive correlation between their skill gains and changes in stiffness during training trials. Mean values of correlation coefficients over the entire subject population were found to be positive (0.59 and 0.46 for the MD and the FD, respectively). Sign tests were used to confirm the statistical significance of the result ($p < 0.00001$).

The results presented points to a control strategy that increases the stiffness overtime while improving the precision in in the modulation of force. These strongly suggest that an internal model of the movement is created and that force is modulated via impedance control.

Discussion

This paper focused on the upper limb modulation of force and its regulation in case of externally imposed arm motions. The results indicate that during force regulation in predictable environments, mechanical impedance increases while force production becomes more stable and the error in applied force decreases.

It was demonstrated in the literature that increasing the contact force in isometric conditions increases the level of muscle activation and consequently increases the magnitude of stiffness [32]. However, the increase in stiffness shown in the "Results section" of this work is independent of the contact force, which is maintained constant throughout the experiment.

Muscle fatigue is another factor that can influence the modulation of muscle force inducing a decrease of both isometric and isotonic maximal exertable forces. Such reduction of force is usually associated with a simultaneous decrease in muscle stiffness [59,60]. Given the significant increase in stiffness recorded in the present experiment, we can conclude that muscle fatigue is not a factor in the phenomenon we observed.

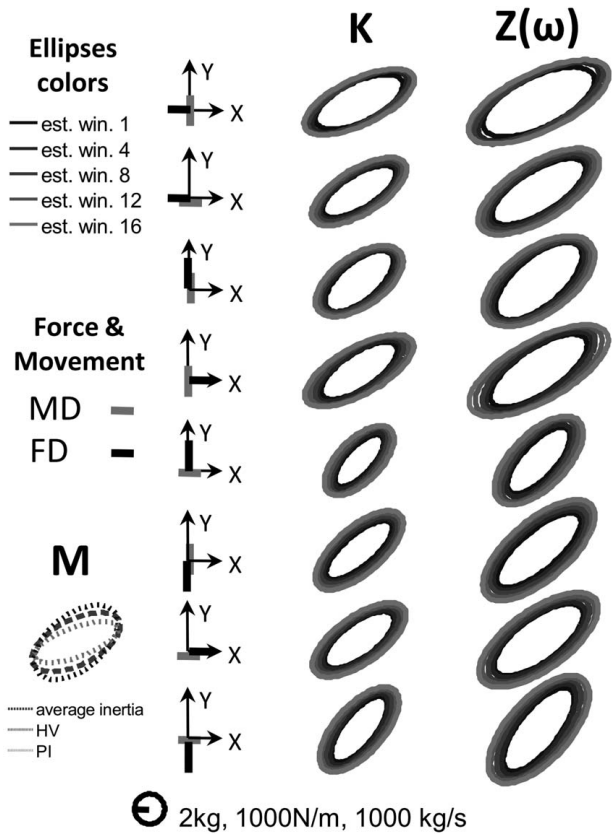

Fig. 6 Ellipses representation for the different components of arm mechanics. M represents the average ellipse of inertia (dashed). The dotted ellipses represent those obtained with the two methods that tend to overestimate (HV) or underestimate (PI) the bulk of inertial properties [53]. Inertial properties are independent of the experimental conditions. For each experimental condition, black segments start from the origin, pointing in the FD. Gray segments lay along the MD and cross the origin. Each component of the ellipse Z(w), is in the form of Eq. (5). Magnitude is calculated for the specific angular frequency of the perturbation $\omega = 2 \cdot \pi \cdot 0.125$[rad/s]. The magnitude of both stiffness and damping are represented for every four estimation windows, according to the color code on the top-left corner.

The observations in this work are valid only for predictable perturbations at the frequency of 0.125 Hz. Different strategies might arise for lower frequencies or nonpredictable environments. However, to render a nonpredictable environment at low frequency appears to be quite challenging as it is easy for the subject to track slowly changing environments [61]. A factor that can influence the stiffness modulations is the predictability of the environment, which depends on the frequency content of the perturbation. When the environment is not predictable, the formation of an internal model is impossible and other strategies need to be employed. Nonetheless, it is difficult to refute that perturbations embedding very low-frequency components are predictable since they are well within the bandwidth of voluntary movements. We used the impedance as a figure of merit for the control schema since it is a variable that can encompass both the intrinsic biomechanics and the neuromuscular control of the arm. Stiffness and damping can be regulated via muscle activations (including co-contraction) and segmental reflexes. On the other hand, the inertial component of the impedance is dictated simply by the geometry of the arm. As the frequency of the movement increases, and with it the unpredictability/entropy of the disturbance [62], the effect of the inertial forces becomes predominant and cannot be modulated by the subject. Therefore, the subject has "no choice" as the impedance will be dominated by the inertial component.

A further question for discussion is to clarify what the influence of visual feedback for force control is. The way in which the task is presented might condition the type of control that the subject chose to utilize. Subjects could try to "remember" the force to be applied, but this is likely prone to the long-term drift. A bias toward a direct control of the position might occur if subjects are responding to visual errors and are trying to drive a cursor to a desired position. We believe that our representation obviates these problems as the origin and target for the force representation vector was independent from the position of the hand. Furthermore, the direction of force application is different than the direction of displacement subjects would have to apply to generate the force. Independent of the control, the direction of contact force and "pushing" direction would coincide only if such direction is also an axis of the endpoint stiffness/compliance ellipse. This might explain a tendency to align the major axis of the stiffness ellipse with the direction of the force.

The findings in this work contradict the intuitive solution described by Eq. (2) (see "Methods section"), which suggests that the impedance of the human arm decreases isotropically as the force production improves. Furthermore, we can discard the hybrid position/force control architecture. The four conditions where force and motion are orthogonal are significant in the context of classical "hybrid position/force control," where the directions of space are separated in mutually orthogonal motion freedoms and force freedoms. This allows the independent specification of which variable is being controlled by the subject and what variables are dictated by the environment (rigid constraint or free space). By using this reasoning, we would expect a decrease in stiffness in the direction of force, which instead did not happen. Conversely, we observed an increase in stiffness/impedance in the general direction of force. Thus, the results are compatible with the idea that the force regulation process employed by the central nervous system involves not only the pure force controller described by Eq. (2) but also a coupled controller mediated via the impedance of the arm. As an adaptation to the environment progresses, an internal model [19] of the environment develops. This model provides the estimates of the kinematic parameters of the environment that drives the coupled motion controller to provide increasingly more accurate feed-forward compensation.

Our results show that stiffness reorientation is toward the direction of the force for each experimental condition, consistent with

Table 2 Influence of window estimates for impedance metrics: three-way (ANOVA) with subject as a random factor and window estimates and inertial models as fixed factors

		1		2		3		4		5		6		7		8	
		F	*p*	F	*p*	F	*p*	F	*p*	F	*p*	F	*p*	F	*p*	F	*p*
K	det(*K*)	13.73	**0.00**	125.3	**0.00**	29.75	**0.00**	126.8	**0.00**	86.91	**0.00**	201.6	**0.00**	97.24	**0.00**	156.4	**0.00**
	ang(*K*)	0.02	0.90	0.01	0.91	4.43	0.06	7.38	0.02	3.49	0.09	0.16	0.70	1.30	0.28	3.21	0.11
Z	det(*Z*)	13.85	**0.00**	125.2	**0.00**	29.78	**0.00**	126.8	**0.00**	86.79	**0.00**	201.7	**0.00**	97.21	**0.00**	156.5	**0.00**
	ang(*Z*)	0.02	0.88	0.01	0.91	4.43	0.06	7.38	0.02	3.50	0.09	0.16	0.70	1.30	0.28	3.21	0.11

$p < 0.01$ is indicated in bold.

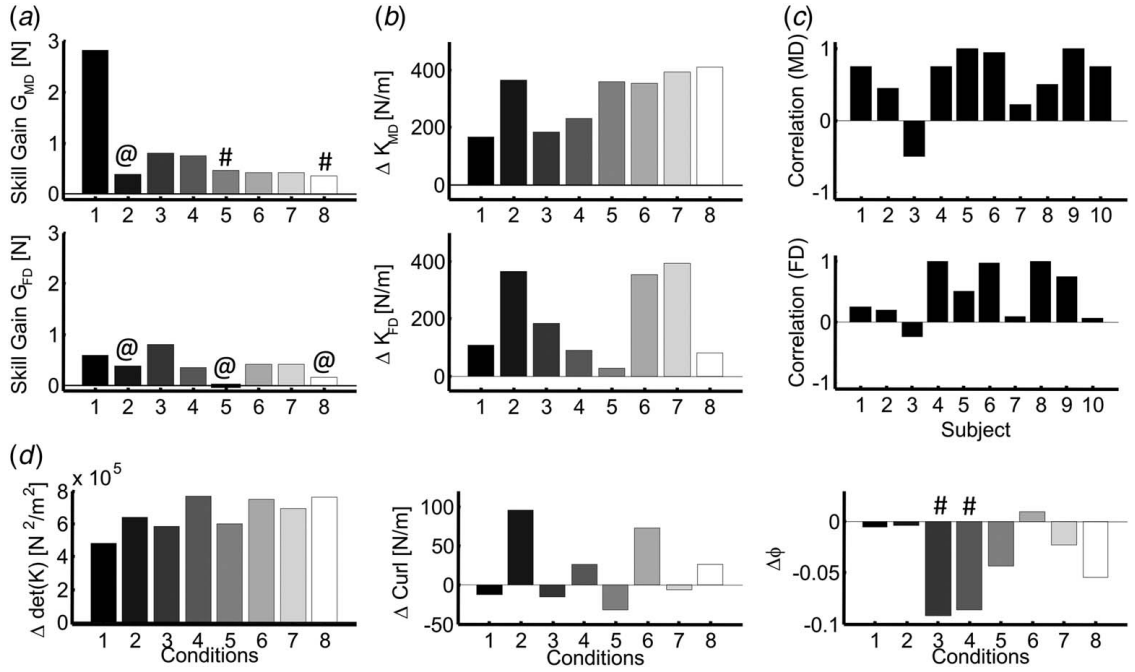

Fig. 7 Average of all subjects and all inertial models. (*a*) Skill gain in the direction of motion G_M and in the direction of force G_F. Nonmarked bars are significant ($p < 0.01$), "#" indicates elements that are marginally significant ($0.01 < p < 0.08$), and "@" indicates the nonsignificant cases. (*b*) Difference in stiffness between the first and the last window estimate. All variations are statistically significant. (c) Correlation between skill gains and changes in stiffness during training trials for each subject. Mean values of correlation coefficients over the entire subject population were positive (0.59 and 0.46 for the MD and the FD, respectively). (*d*) Change in metrics of the stiffness matrix for each condition. Changes in determinant are all significant ($p < 0.01$). Changes in curl and orientation are not significant; "#" indicates marginally significant change in orientation ($0.01 < p < 0.08$).

the previous results for isometric conditions [29,62–65]. Note that the initial orientation of stiffness is different for each experimental condition, such as leaning toward the force direction (FD) and not changing during training. This is consistent with the predictive properties of the motor plan [66,67]. This observation points out that subjects already start with the preplanned strategy of position control where force is generated, by modulating the stiffness. A general increase in stiffness might be necessary to increase the tracking capabilities of the external disturbance. If subjects can predict what the robot trajectory will be, a higher stiffness about that trajectory will stabilize the motion against unpredictable perturbations and improve the tracking. Hence, when the movement is well tracked, a bias of the predicted trajectory can generate the desired target force with increased stiffness. Applying a bias displacement in the direction of the force will result in a force generated in the same direction only if one of the stiffness ellipse's axes is oriented in the same direction. Thus, if the behavior is preplanned, a convenient strategy is to re-orient, from the beginning of the exercise, the major axis of the stiffness ellipse in the direction of the applied force. This strategy achieves smaller amplitude bias pointing in the desired direction. Even though the alignment of the stiffness ellipse is not perfect, the rotation of the stiffness seems to be preselected at the beginning of each trial and does not statistically change during it as a consequence of adaptation.

Table 3 Statistical difference between *xy* and *yx* terms

	1		2		3		4		5		6		7		8	
	F	*p*	F	*p*	F	*p*	F	*p*	F	*p*	F	*p*	F	*p*	F	*p*
K	0.80	0.39	0.16	0.70	0.41	0.54	0.81	0.39	0.60	0.45	1.12	0.32	0.39	0.55	0.41	0.54
Z	0.77	0.40	0.15	0.70	0.39	0.54	0.80	0.39	0.59	0.46	1.11	0.32	0.39	0.55	0.41	0.54

Note: Analysis of variance with subject and session as random factors and method as a fixed factor for impedance CURL ($p < 0.01$).

Table 4 *p* values for repeated measure MANCOVA among subjects and methods between first and last session of each exercise

	K								*Z*							
	Trials►								Trials►							
xx	**0.00**	**0.00**	**0.00**	**0.00**	**0.00**	**0.00**	**0.00**	**0.00**	**0.00**	**0.00**	**0.00**	**0.00**	**0.00**	**0.00**	**0.00**	**0.00**
xy	0.04	0.03	0.05	0.03	0.87	**0.01**	0.04	0.24	0.07	0.04	**0.00**	**0.00**	0.05	**0.00**	0.11	0.34
yx	**0.01**	0.62	0.09	0.05	0.64	0.25	0.23	0.35	0.02	0.11	**0.00**	0.12	0.89	0.36	0.38	0.59
yy	**0.00**	**0.00**	**0.00**	**0.00**	**0.00**	**0.00**	**0.00**	**0.00**	0.16	**0.00**	0.65	**0.00**	**0.00**	**0.00**	**0.00**	**0.00**

$p < 0.01$ is indicated in bold.

Since the applied force diminishes, while the stiffness increases, this behavior is compatible with a decrease in bias displacement to generate the desired force. If the displacement is progressively smaller, subjects can concentrate on compensating the external movement, while letting the stiffness modulation satisfy the required output of force. Furthermore, the increase of stiffness without a rotation of the ellipses during each condition suggests that its modulation occurs by co-contraction [68]. This is also supported by the absence of statistically significant curl.

Conclusions

We believe that in order to properly plan a robotic control strategy, it is necessary to understand how the "mechanical load" applied to the robot's end effector changes. In this case, the "mechanical load" is the human acting as an actively controlled physical system and adapting to the interaction force and movements of the robot's end effector. The present paper provides the useful insight that humans use a predictive internal model constructing a trajectory and modulating their impedance, increasing it over time. Thus, to guarantee the safety of the physical human–robot interaction, changes in the trajectory of the robot's end effector need to be carefully controlled when humans are applying a load to it over time. In fact, since the stiffness of the individual increases over time, a sudden change in trajectory in the direction of the major axis of the subject's stiffness ellipse will generate peak forces that are much higher over time when compared with sudden movements in the direction orthogonal to it.

Acknowledgment

This work was supported by NINDS (Grant No. 2R01NS035673; Funder ID: 10.13039/100000065), by the 2016 Cooney-Jackman Endowed Professorships and by the Dr. and Mrs. Arthur William Phillips Charitable Trust.

Appendix A

Restricting our example to a one-dimensional case, the mechanical impedance of the arm and environment, defined in the complex plane as the ratio between the Laplace transform of force and velocity [7,69] is as follows:

$$Z(s) = B + \frac{K}{s} + sM \tag{A1}$$

$$Z_e(s) = B_e + \frac{K_e}{s} + sM_e \tag{A2}$$

where $s = \alpha + j\omega$ represents a complex number that includes the angular frequency of the motion ω. Assuming for simplicity, the scalar form of Eqs. (3) and (4) in the frequency domain, and substituting for Eqs. (A1) and (A2), we obtain

$$sM_e v + Z_e \cdot (v_e - v) = F \tag{A3}$$

$$sMv_{\text{ref}} + Z \cdot (v - v_{\text{ref}}) + F_{\text{ref}} = F \tag{A4}$$

where the dependency of Z and Z_e on s is omitted to streamline the notation. The impedance Z_e is imposed as a control variable of the robot, and therefore, it is invariant within a given environment. On the other hand, the impedance of the arm Z and the transform of reference force and reference velocity v_{ref} and F_{ref}, respectively, are parameters that can be modified by the CNS.

We will demonstrate in "Results section" that the inertial components of both the environment and the arm impedance are negligible with respect to the total impedance (i.e., $sM_e \ll Z_e$, $sM \ll Z$). This allows us to omit such term from Eqs. (A3) and (A4). Thus, after such approximation, by equating Eqs. (A3) and (A4) and isolating for $(v_e - v)$, we have

$$(v_e - v) = \frac{Z \cdot (v - v_{\text{ref}}) + F_{\text{ref}}}{Z_e} \tag{A5}$$

It easy to see that

$$(v_e - v_{\text{ref}}) = (v_e - v) + (v - v_{\text{ref}}) \tag{A6}$$

Therefore, substituting Eq. (A6) into Eq. (A5), we have

$$(v_e - v_{\text{ref}}) = \frac{Z \cdot (v - v_{\text{ref}}) + F_{\text{ref}}}{Z_e} + (v - v_{\text{ref}}) \tag{A7}$$

Isolating $(v - v_{\text{ref}})$, we obtain

$$(v - v_{\text{ref}}) = \frac{Z_e}{Z_e + Z} \cdot (v_e - v_{\text{ref}}) - \frac{F_{\text{ref}}}{Z_e + Z} \tag{A8}$$

Thus, substituting Eq. (A8) in Eq. (A5) gives

$$F = \frac{Z_e}{Z_e + Z} \cdot (Z \cdot (v_e - v_{\text{ref}}) + F_{\text{ref}}) \tag{A9}$$

By using Eq. (A9), we can analyze different force regulation strategies to obtain $F = F_{\text{ref}}$.

Appendix B

Measure Validation on a Mechanical Prototype. While the canonical correlation assesses the assumption of a system's linearity, it does not convey a measure of how precise the estimation is. To assess the validity of the aforementioned procedure with respect to our experimental apparatus, we estimated the stiffness of a custom-made mechanical rig. Anisotropic stiffness and isotropic endpoint inertia were replicated with a set of calibrated springs and masses. The rig's stiffness was first measured at a steady state using a single DOF load cell and a noncontact optical system to check the load cell alignment and spring displacements. Stiffness was observed to be $\mathbf{K}_{basic} = \begin{bmatrix} 615 & 0 \\ 0 & 507 \end{bmatrix}$ N/m. Test mass was set at $M_{basic} = 1.87$ kg. We employed a passive damper to attenuate the vibration of the springs outside the plane of perturbation, thus suppressing the modes that could not be accounted for by our planar model. The damper consisted of a series of thin rubber sheets, positioned on top of the springs to dissipate the out-of-plane vibrational energy (see Fig. 8).

The mechanical rig was subject to the same perturbations as the subject. The inertial properties of the rig were evaluated

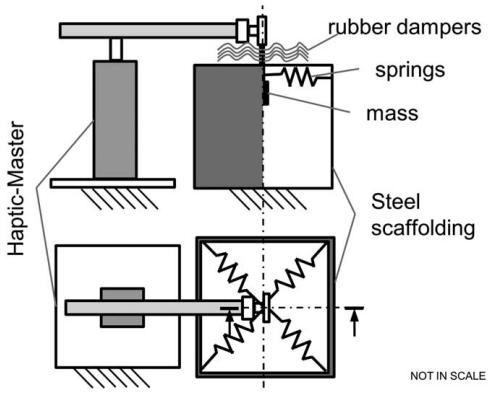

Fig. 8 Graphical representation of the mechanical rig used for validating the regressive technique. Rubber sheets were placed on top of the springs to limit their out-of-plane oscillations. The vibrational energy dissipated by the rubber oscillation produced a slight damping effect.

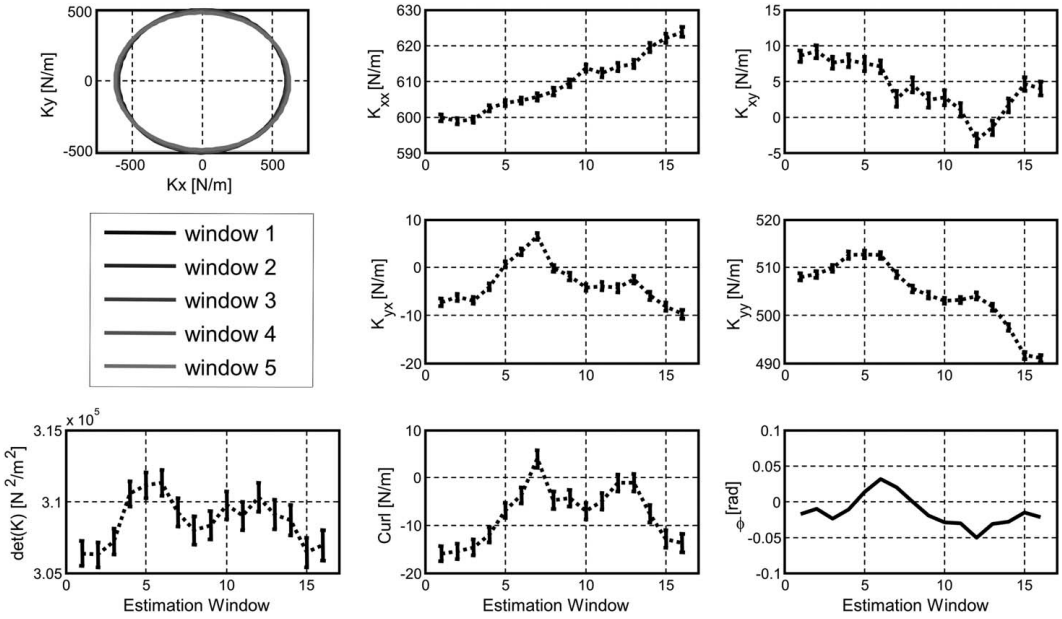

Fig. 9 Stiffness features of the experimental apparatus. Each coefficient estimation presents a small drift, which is never bigger than ±2.7%. Estimations of the stiffness metrics also present some drift, but do not have a preferential direction.

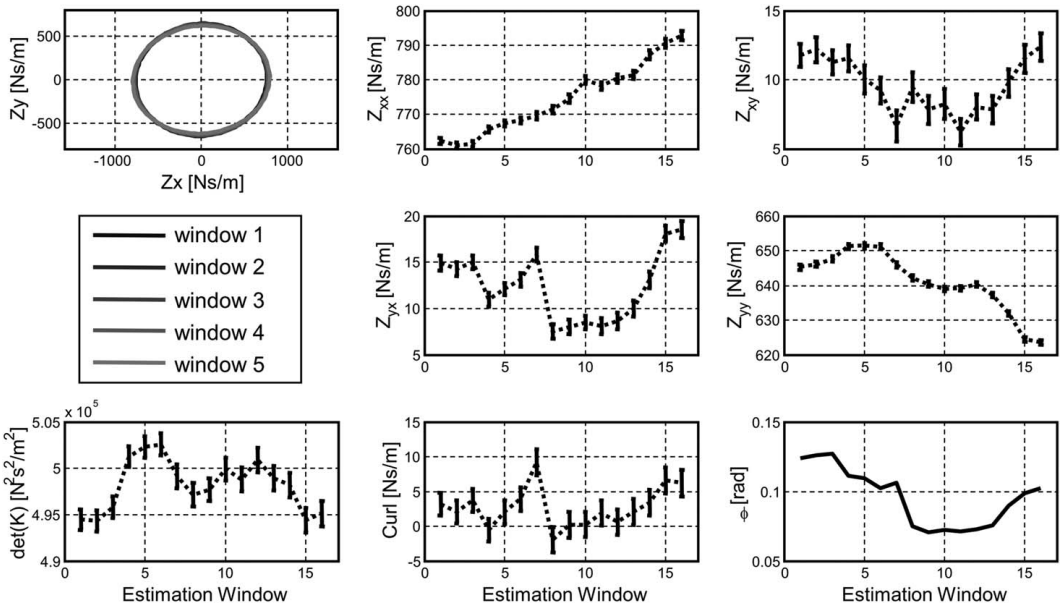

Fig. 10 Estimated impedance of the mechanical rig

separately, and a full regression was used to estimate stiffness and damping.

Statistical Testing. By using MANCOVA on both stiffness and damping, we monitored for each of the five repetitions of the task if the estimated coefficients outside of the diagonal were statistically different to each other for each window estimate. Moreover, we tested the statistical difference of each coefficient between the first and the last window estimate. Subsequently, we used an ANOVA to evaluate the influence of each window estimate on the mean determinant and matrix rotation among the five repetitions of the task.

Reliability of the Impedance Estimate. Results for stiffness and impedance estimations are presented in Figs 9 and 10. Stiffness estimates obtained with the implemented regression technique gave results consistent within ±2.7% of $\mathbf{K}_{basic} = \begin{bmatrix} 615 & 0 \\ 0 & 507 \end{bmatrix}$ N/m (see "Methods section"). The canonical correlation for the regression on the mechanical apparatus was quite high, giving an $r_I^2 = 0.96$. Hence, the linear component of elastic force in the analyzed system is predominant.

Table 5 shows no stiffness and impedance curl for all the 16 window estimates as expected for a passive mechanical rig. Table 6 shows no statistical difference of the stiffness matrix coefficients between the first and the last window estimate for all five repetitions of the measure cycle. ANOVAs on determinant and orientation of the rig's stiffness matrix did not show any significant change between the averages of the first and the last window estimates ($F = 0.05$, $p > 0.99$).

Table 5 Curl significance for the mechanical rig obtained using a multivariate analysis of covariance

	K					*Z*				
Windows▼	Repetitions ►					Repetitions ►				
1	0.85	0.87	0.93	0.84	0.95	1.00	0.75	0.94	0.98	0.91
2	0.89	0.64	0.81	0.83	0.98	0.97	0.71	0.88	0.88	1.00
3	0.85	0.89	0.94	0.98	0.93	0.83	0.89	0.91	0.94	0.93
4	0.45	0.97	0.73	0.70	0.75	0.69	0.98	0.81	0.76	0.75
5	0.90	0.77	0.91	0.87	0.81	0.93	0.77	0.91	0.94	0.83
6	0.93	0.86	0.97	0.93	0.83	0.81	0.96	0.91	0.92	0.81
7	0.59	0.79	0.83	0.86	0.87	0.64	0.67	0.80	0.80	0.86
8	0.52	0.75	0.83	0.66	0.80	0.62	0.77	0.86	0.73	0.78
9	0.64	0.76	0.93	0.86	0.87	0.68	0.85	0.98	0.90	0.87
10	0.74	0.81	0.97	0.95	0.99	0.70	0.71	0.98	0.97	0.99
11	0.59	0.87	0.92	0.86	0.99	0.69	0.87	0.95	0.92	1.00
12	0.74	0.88	0.92	0.95	0.99	0.63	0.80	0.98	0.92	1.00
13	0.59	0.76	0.96	0.96	0.81	0.51	0.57	0.90	0.83	0.83
14	0.47	0.71	0.90	0.88	0.78	0.64	0.79	0.99	0.99	0.74
15	0.67	0.88	0.83	0.94	0.92	0.55	0.72	0.99	0.94	0.93
16	0.47	0.68	0.96	0.98	0.79	0.50	0.67	0.94	0.83	0.78

Note: The table reports a p value smaller than 0.01 if the term outside the diagonal of the stiffness (K) and impedance (Z) matrices are statistically different. For both K and Z, the curl is never significant as is expected for a passive system.

Table 6 *P* values smaller than 0.01 if the term of the stiffness (*K*) and impedance (*Z*) matrices are statistically different between the first and the last estimation windows (MANCOVA)

	K					*Z*				
	Estimations►					Estimations►				
xx	0.07	0.05	0.37	0.36	0.40	0.58	0.4	0.16	0.97	0.49
xy	0.65	0.53	0.22	0.16	0.04	0.64	0.5	0.26	0.2	0.46
yx	0.77	0.90	0.46	0.82	0.47	0.69	0.76	0.95	0.63	0.78
yy	0.34	0.96	0.18	0.03	0.41	0.45	0.54	0.93	0.33	0.82

Note: Even though the effect of the rubber dampers is slightly nonlinear, there is no significant hysteretic effect on the overall impedance.

Given the results obtained with the calibrated mechanical rig, we can infer that since the stiffness variations monitored in the human subjects were larger than 2.7%, it is quite unlikely that these would be generated as an artifact of the technique itself or by noisy estimates.

References

[1] Buneo, C. A., and Andersen, R. A., 2006, "The Posterior Parietal Cortex: Sensorimotor Interface for the Planning and Online Control of Visually Guided Movements," Neuropsychologia, **44**(13), pp. 2594–2606.

[2] Georgopoulos, A., Ashe, J., Smyrnis, N., and Taira, M., 1992, "The Motor Cortex and the Coding of Force," Science, **256**(5064), pp. 1692–1695.

[3] Hamel-Pâquet, C., Sergio, L. E., and Kalaska, J. F., 2006, "Parietal Area 5 Activity Does Not Reflect the Differential Time-Course of Motor Output Kinetics During Arm-Reaching and Isometric-Force Tasks," J. Neurophysiol., **95**(6), pp. 3353–3370.

[4] Sergio, L. E., and Kalaska, J. F., 1998, "Changes in the Temporal Pattern of Primary Motor Cortex Activity in a Directional Isometric Force Versus Limb Movement Task," J. Neurophysiol., **80**(3), pp. 1577–1583.

[5] Torres, E., and Andersen, R., 2006, "Space Time Separation During Obstacle-Avoidance Learning in Monkeys," J. Neurophysiol., **96**(5), pp. 2613–2632.

[6] Raibert, M. H., and Craig, J. J., 1981, "Hybrid Position/Force Control of Manipulators," J. Dyn. Syst. Meas. Control, **103**(2), pp. 126–133.

[7] Hogan, N., 1985, "Impedance Control: An Approach to Manipulation. Parts I, II, III," J. Dyn. Syst. Meas. Control, **107**(1), pp. 1–24.

[8] Mason, M. T., 1986, "Mechanics and Planning of Manipulator Pushing Operations," Int. J.Rob. Res., **5**(3), pp. 53–71.

[9] Yoshikawa, T., 1987, "Dynamic Hybrid Position/Force Control of Robot Manipulators–Description of Hand Constraints and Calculation of Joint Driving Force," Rob. Autom. IEEE J., **3**(5), pp. 386–392.

[10] Pratt, G. A., and Williamson, M. M., 1995, "Series Elastic Actuators," Proceedings 1995 IEEE/RSJ International Conference on Intelligent Robots and Systems, Pittsburgh, PA, Aug. 5–9, pp. 399–406, Vol. 391.

[11] Mason, M. T., 1981, "Compliance and Force Control for Computer Controlled Manipulators," IEEE Trans. Syst. Man Cybern., **11**(6), pp. 418–432.

[12] Mussa-Ivaldi, F. A., Hogan, N., and Bizzi, E., 1985, "Neural, Mechanical, and Geometric Factors Subserving arm Posture in Humans," J. Neurosci., **5**(10), pp. 2732–2732.

[13] Burdet, E., Osu, R., Franklin, D. W., Milner, T. E., and Kawato, M., 2001, "The Central Nervous System Stabilizes Unstable Dynamics by Learning Optimal Impedance," Nature, **414**(6862), pp. 446–449.

[14] Mitrovic, D., Klanke, S., Osu, R., Kawato, M., and Vijayakumar, S., 2010, "A Computational Model of Limb Impedance Control Based on Principles of Internal Model Uncertainty," PLoS One, **5**(10), p. e13601.

[15] Chib, V. S., Krutky, M. A., Lynch, K. M., and Mussa-Ivaldi, F. A., 2009, "The Separate Neural Control of Hand Movements and Contact Forces," J. Neurosci., **29**(12), pp. 3939–3947.

[16] Cianchetti, F. A., and Valero-Cuevas, F. J., 2010, "Anticipatory Control of Motion-to-Force Transitions With the Fingertips Adapts Optimally to Task Difficulty," J. Neurophysiol., **103**(1), pp. 108–116.

[17] Mugge, W., Abbink, D. A., Schouten, A. C., Dewald, J. P. A., and van der Helm, F. C. T., 2010, "A Rigorous Model of Reflex Function Indicates That Position and Force Feedback Are Flexibly Tuned to Position and Force Tasks," Exp. Brain Res., **200**(3–4), pp. 325–340.

[18] Wong, J., Wilson, E. T., Malfait, N., and Gribble, P. L., 2009, "Limb Stiffness is Modulated With Spatial Accuracy Requirements During Movement in the Absence of Destabilizing Forces," J. Neurophysiol., **101**(3), pp. 1542–1549.

[19] Shadmehr, R., and Mussa-Ivaldi, F., 1994, "Adaptive Representation of Dynamics During Learning of a Motor Task," J. Neurosci., **14**(5), pp. 3208–3224.

[20] Lackner, J. R., and Dizio, P., 1994, "Rapid Adaptation to Coriolis Force Perturbations of Arm Trajectory," J. Neurophysiol., **72**(1), pp. 299–313.

[21] Guigon, E., Baraduc, P., and Desmurget, M., 2007, "Coding of Movement- and Force-Related Information in Primate Primary Motor Cortex: A Computational Approach," Eur. J. Neurosci., **26**(1), pp. 250–260.

[22] Intveld, R. W., Dann, B., Michaels, J. A., and Scherberger, H., 2018, "Neural Coding of Intended and Executed Grasp Force in Macaque Areas AIP, F5, and M1," Sci. Rep., **8**(1), p. 17985.

[23] Cowper-Smith, C. D., Lau, E. Y. Y., Helmick, C. A., Eskes, G. A., and Westwood, D. A., 2010, "Neural Coding of Movement Direction in the Healthy Human Brain," PLoS One, **5**(10), p. e13330.

[24] Tankus, A., Yeshurun, Y., Flash, T., and Fried, I., 2009, "Encoding of Speed and Direction of Movement in the Human Supplementary Motor Area," J. Neurosurg., **110**(6), pp. 1304–1316.

[25] Ferrari-Toniolo, S., Visco-Comandini, F., Papazachariadis, O., Caminiti, R., and Battaglia-Mayer, A., 2015, "Posterior Parietal Cortex Encoding of Dynamic Hand Force Underlying Hand–Object Interaction," J. Neurosci., **35**(31), p. 10899.

[26] Osu, R., and Gomi, H., 1999, "Multijoint Muscle Regulation Mechanisms Examined by Measured Human Arm Stiffness and EMG Signals," J. Neurophysiol., **81**(4), pp. 1458–1468.

[27] Flash, T., and Mussa-Ivaldi, F., 1990, "Human Arm Stiffness Characteristics During the Maintenance of Posture," Exp. Brain Res., **82**(2), pp. 315–326.

[28] Weiss, P. L., Hunter, I. W., and Kearney, R. E., 1988, "Human Ankle Joint Stiffness Over the Full Range of Muscle Activation Levels," J. Biomech., **21**(7), pp. 539–544.

[29] Darainy, M., Malfait, N., Gribble, P. L., Towhidkhah, F., and Ostry, D. J., 2004, "Learning to Control Arm Stiffness Under Static Conditions," J. Neurophysiol., **92**(6), pp. 3344–3350.

[30] Shin, D., Kim, J., and Koike, Y., 2009, "A Myokinetic Arm Model for Estimating Joint Torque and Stiffness From EMG Signals During Maintained Posture," J. Neurophysiol., **101**(1), pp. 387–401.

[31] Osu, R., Franklin, D. W., Kato, H., Gomi, H., Domen, K., Yoshioka, T., and Kawato, M., 2002, "Short- and Long-Term Changes in Joint Co-Contraction Associated With Motor Learning as Revealed From Surface EMG," J. Neurophysiol., **88**(2), pp. 991–1004.
[32] Perreault, E. J., Kirsch, R. F., and Crago, P. E., 2001, "Effects of Voluntary Force Generation on the Elastic Components of Endpoint Stiffness," Exp. Brain Res., **141**(3), pp. 312–323.
[33] Gribble, P. L., Mullin, L. I., Cothros, N., and Mattar, A., 2003, "Role of Cocontraction in Arm Movement Accuracy," J. Neurophysiol., **89**(5), pp. 2396–2405.
[34] Piovesan, D., Pierobon, A., DiZio, P., and Lackner, J. R., 2013, "Experimental Measure of Arm Stiffness During Single Reaching Movements With a Time-Frequency Analysis," J. Neurophysiol., **110**(10), pp. 2484–2496.
[35] van der Linde, R. Q., and Lammertse, P., 2003, "HapticMaster—A Generic Force Controlled Robot for Human Interaction," Ind. Robot Int. J., **30**(6), pp. 515–524.
[36] Craig, J. J., and Raibert, M., 1979, "A Systematic Method of Hybrid Position/Force Control of a Manipulator," COMPSAC 79. Proceedings. Computer Software and The IEEE Computer Society's Third International Applications Conference, 1979, Chicago, IL, Nov. 6–8, pp. 446–451.
[37] Jingguo, W., and Yangmin, L., 2010, "Hybrid Impedance Control of a 3-DOF Robotic Arm Used for Rehabilitation Treatment," 2010 IEEE Conference on Automation Science and Engineering (CASE), Toronto, ON, Canada, Aug. 21–24, pp. 768–773.
[38] Gomi, H., and Kawato, M., 1997, "Human Arm Stiffness and Equilibrium-Point Trajectory During Multi-Joint Movement," Biol. Cybern., **76**(3), pp. 163–171.
[39] Piovesan, D., Pierobon, A., DiZio, P., and Lackner, J. R., 2012, "Measuring Multi-Joint Stiffness During Single Movements: Numerical Validation of a Novel Time-Frequency Approach," PLoS One, **7**(3), p. e33086.
[40] Burdet, E., Osu, R., Franklin, D. W., Milner, T. E., and Kawato, M., 1999, "Measuring Stiffness During Arm Movements in Various Dynamic Environments," Annual Symposium on Haptic Interfaces and Virtual Environments for Teleoperator Systems, Nashville, TN, Nov. 14–19, pp. 421–428.
[41] Dietz, V., Trippel, M., and Berger, W., 1991, "Reflex Activity and Muscle Tone During Elbow Movements in Patients With Spastic Paresis," Ann. Neurol., **30**(6), pp. 767–779.
[42] Given, J. D., Dewald, J. P. A., and Rymer, W. Z., 1995, "Joint Dependent Passive Stiffness in Paretic and Contralateral Limbs of Spastic Patients With Hemiparetic Stroke,"J. Neurol., Neurosurg. Psychiatry, **59**(3), pp. 271–279.
[43] Mirbagheri, M. M., Barbeau, H., and Kearney, R. E., 2000, "Intrinsic and Reflex Contributions to Human Ankle Stiffness: Variation With Activation Level and Position," Exp. Brain Res., **135**(4), pp. 423–436.
[44] Mirbagheri, M. M., Harvey, R., and Rymer, W. Z., 2002, "Mechanical Properties of the Elbow Joint in Spastic Hemiparetic Stroke Subjects," Proceedings of the Second Joint 24th Annual Conference and the Annual Fall Meeting of the Biomedical Engineering Society Engineering in Medicine and Biology, Houston, TX, Oct. 23–26, pp. 2449–2450.
[45] Galiana, L., Fung, J., and Kearney, R., 2005, "Identification of Intrinsic and Reflex Ankle Stiffness Components in Stroke Patients," Exp. Brain Res., **165**(4), pp. 422–434.
[46] Dolan, J. M., Friedman, M. B., and Nagurka, M. L., 1993, "Dynamic and Loaded Impedance Components in the Maintenance of Human arm Posture," IEEE Trans. Syst. Man Cybern., **23**(3), pp. 698–709.
[47] Hanavan, E. P. J., 1964, *A Mathematical Model of the Human Body*, Wright-Patterson Air Force Base, Dayton, OH.
[48] Dempster, W. T., 1955, "Space Requirements of the Seated Operator. Geometrical, Kinematic, and Mechanical Aspects of the Body With Special Reference to the Limbs," No. 159, Wright Air Development, Dayton, OH.
[49] Chandler, R. F., Clauser, C. E., McConville, J. T., Reynolds, H. M., and Young, J. W., 1975, *Investigation of Inertial Properties of the Human Body*, Wright-Patterson Air Force Base, Dayton, OH.
[50] Clauser, C. E., McConville, J. T., and Young, J. W., 1969, "Weight, Volume, and Center of Mass of Segments of the Human Body," No. 70, Wright-Patterson Air Force Base, Dayton, OH.
[51] McConville, J. T., Churchill, T. D., Kaleps, I., Clauser, C. E., and Cuzzi, J., 1980, "Anthropometric Relationships of Body and Body Segment Moments of Inertia," Wright-Patterson Air Force Base, Dayton, OH.
[52] Zatsiorsky, V., and Seluyanov, V., 1983, "The Mass and Inertia Characteristics of the Main Segments of the Human Body 30," *International Congress of Biomechanics: Biomechanics VIII-B*, H. A. K. K. Matsui, ed., Human Kinetics, Champaign, IL, pp. 1152–1159.
[53] Piovesan, D., Pierobon, A., DiZio, P., and Lackner, J. R., 2011, "Comparative Analysis of Methods for Estimating Arm Segment Parameters and Joint Torques From Inverse Dynamics," ASME J. Biomech. Eng., **133**(3), p. 031003.
[54] Zatsiorsky, V. M., 2002, "Best Predictive Regression Equations for Estimating Inertial Properties of Body Segments in Males, Appendix A2.8," *Kinetics of Human Motion*, V. M. Zatsiorsky, ed., Human Kinetics, Champain, IL, pp. 600–601.
[55] de Leva, P., 1996, "Adjustments to Zatsiorsky-Seluyanov's Segment Inertia Parameters," J. Biomech., **29**(9), pp. 1223–1230.
[56] Rencher, A. C., 2002, *Methods of Multivariate Analysis, Second Edition*, John Wiley & Sons, Inc., New York.
[57] Press, W. H., Flannery, B. P., Teukolsky, S. A., and Vetterling, W. T., 1992, *Numerical Recipes in C: The Art of Scientific Computing*, Cambridge University Press, Cambridge, UK.
[58] Darainy, M., Towhidkhah, F., and Ostry, D. J., 2007, "Control of Hand Impedance Under Static Conditions and During Reaching Movement," J. Neurophysiol., **97**(4), pp. 2676–2685.
[59] Avela, J., 1998, "Interaction Between Muscle Stiffness and Stretch Reflex Sensitivity After Long-Term Stretch-Shortening Cycle Exercise," Muscle Nerve, **21**(9), pp. 1224–1227.
[60] Toumi, H., Poumarat, G., Best, T. M., Martin, A., Fairclough, J., and Benjamin, M., 2006, "Fatigue and Muscle–Tendon Stiffness After Stretch–Shortening Cycle and Isometric Exercise," Appl. Physiol. Nutr. Metab., **31**(5), pp. 565–572.
[61] Piovesan, D., Pierobon, A., and Mussa Ivaldi, F. A., 2013, "Critical Damping Conditions for Third Order Muscle Models: Implications for Force Control," ASME J. Biomech. Eng., **135**(10), p. 101010.
[62] Piovesan, D., Morasso, P., Giannoni, P., and Casadio, M., 2013, "Arm Stiffness During Assisted Movement After Stroke: The Influence of Visual Feedback and Training," IEEE Trans. Neural Syst. Rehabil. Eng., **21**(3), pp. 454–465.
[63] Gomi, H., and Osu, R., 1998, "Task-Dependent Viscoelasticity of Human Multijoint Arm and Its Spatial Characteristics for Interaction With Environments," J. Neurosci., **18**(21), pp. 8965–8978.
[64] Gribble, P. L., Ostry, D. J., Sanguineti, V., and Laboissière, R., 1998, "Are Complex Control Signals Required for Human Arm Movement?," J. Neurophysiol., **79**(3), pp. 1409–1424.
[65] Piovesan, D., Casadio, M., Mussa-Ivaldi, F. A., and Morasso, P. G., 2011, "Multijoint Arm Stiffness During Movements Following Stroke: Implications for Robot Therapy," 2011 IEEE International Conference on Rehabilitation Robotics (ICORR), Zurich, Switzerland, June 27–July 1, pp. 1–7.
[66] Pigeon, P., Bortolami, S. B., DiZio, P., and Lackner, J. R., 2003, "Coordinated Turn-and-Reach Movements. I. Anticipatory Compensation for Self-Generated Coriolis and Interaction Torques," J. Neurophysiol., **89**(1), pp. 276–289.
[67] Pigeon, P., Bortolami, S. B., DiZio, P., and Lackner, J. R., 2003, "Coordinated Turn-and-Reach Movements. II. Planning in an External Frame of Reference," J. Neurophysiol., **89**(1), pp. 290–303.
[68] Piovesan, D., Morasso, P., Giannoni, P., and Casadio, M., 2012, "Arm Stiffness During Assisted Movement After Stroke: The Influence of Visual Feedback And Training," IEEE Trans. Neural Syst. Rehabil. Eng., **21**(3), pp. 454–465.
[69] Findeisen, D., 2000, *System Dynamics and Mechanical Vibrations: An Introduction*, Springer, Berlin.